Electronic Supplementary Material (ESI) for Nanoscale.

This updated version of the Electronic Supplementary Information (published on 05 Nov 2018) replaces the original version first published on-line on 23 Sep 2016.

Supporting Information:

Hierarchical Porous Nitrogen-Rich Carbon Nanospheres with High and Durable Capabilities for Lithium and Sodium Storage

Lianbo Ma,[a#] Renpeng Chen,[a#] Yi Hu,[a] Guoyin Zhu,[a] Tao Chen,[a] Hongling Lu,[a] Jia Liang,[a] Zuoxiu Tie,[a,b] Zhong Jin,[*a] and Jie Liu[*a,c]

[a] Key Laboratory of Mesoscopic Chemistry of MOE and Collaborative Innovation Center of Chemistry for Life Sciences, School of Chemistry and Chemical Engineering, Nanjing University, Nanjing, Jiangsu 210093, China

[b] College of Engineering and Applied Sciences, Nanjing University, Nanjing, Jiangsu 210093, China

[c] Department of Chemistry, Duke University, Durham, North Carolina, 27708, USA

[#]These authors contributed equally to this work.

[*]Address correspondence to: zhongjin@nju.edu.cn (Prof. Z. Jin); j.liu@duke.edu (Prof. J. Liu)

Table S1. Comparison of lithium storage performance of HPNC material with other pristine or nitrogen-doped carbon-based materials in the literatures [24,26,28,39–52].

Ref.	Samples	Nitrogen content	Current density (mA g^{-1})	Cycle number	Specific capacity after cycling (mAh g^{-1})	Retention from the second cycle (%)
This work	**Hierarchical porous nitrogen-rich carbon nanospheres**	**17.4 wt.% (15.3 at.%)**	**100**	**100**	**1,187**	**104.7**
			1,000	**500**	**788**	**82.8**
			5,000	**1,000**	**396**	**84.4**
24	Porous carbon fiber	--	186	45	400	~100
26	Hollow carbon nanospheres	--	37	50	630	74.1
28	Graphene nanosheets	--	50	20	600	80.0
39	Hollow carbon nanospheres	--	186	100	~400	81.6
40	Nitrogen-doped porous graphene	5.8 at.%	400	200	496	108.3
41	Branched graphene nanocapsules	2.8 at.%	500	200	1,373	95.3
42	Nitrogen-doped graphene	3.9 at.%	74	50	550	57.9
43	Folded structured graphene	--	100	100	568	78.9
44	Nitrogen-doped carbon nanotube	16.4 at.%	100	100	397	82.7
45	Nitrogen-doped carbon capsules	13.0 at.%	50	50	1,046	95.1
46	Nitrogen-doped graphene/graphite foam	2~3 at.%	186	300	397	94.5
47	3D nitrogen-doped graphene@CNT	2.5 at.%	2,000	300	1,089	72.6
48	Hollow CNT/carbon fiber	1.4 wt.%	100	70	1,150	76.6
49	Nitrogen-doped graphene sheets	23.6 wt.%	100	108	770	96.3
50	Nitrogen-doped porous carbon	2.1 wt.%	100	160	1,336	89.1
51	Graphene nanosheets	--	1,000	300	557	92.8
52	2D carbon nanosheets	--	100	10	~600	57.7

Table S2. Comparison of sodium storage performance of HPNC material with other pristine or nitrogen-doped carbon-based materials in the literatures [23,25,27,53–62].

Ref.	Samples	Nitrogen content	Current density (mA g^{-1})	Cycle number	Specific capacity after cycling (mAh g^{-1})
This work	**Hierarchical porous nitrogen-rich carbon nanospheres**	**17.4 wt.% (15.3 at.%)**	**100**	**100**	**272**
			1,000	**500**	**136**
23	Hollow carbon nanowires	--	50	400	251
25	Carbon fibers	--	50	280	245
27	Hollow carbon nanospheres	--	100	100	160
53	Nitrogen-rich porous carbon	7.8 at.%	500	800	~110
54	Mesocarbon microbeads	--	15	50	172
55	Carbon membrane	--	40	200	243
56	Wood fiber derived hard carbon	--	100	200	196
57	Polyvinyl chloride nanofibers derived carbon	--	12	126	211
58	Hierarchical carbon nanocages	--	100	100	~150
59	Graphite	--	200	6,000	110
60	Hydrogen-enriched porous carbon nanosheets	--	50	100	302
61	Nitrogen-doped carbon nanofibers	10.7 wt.%	50	200	254
62	Nitrogen-doped bamboo-like carbon nanotubes	2.5 at.%	500	160	~105

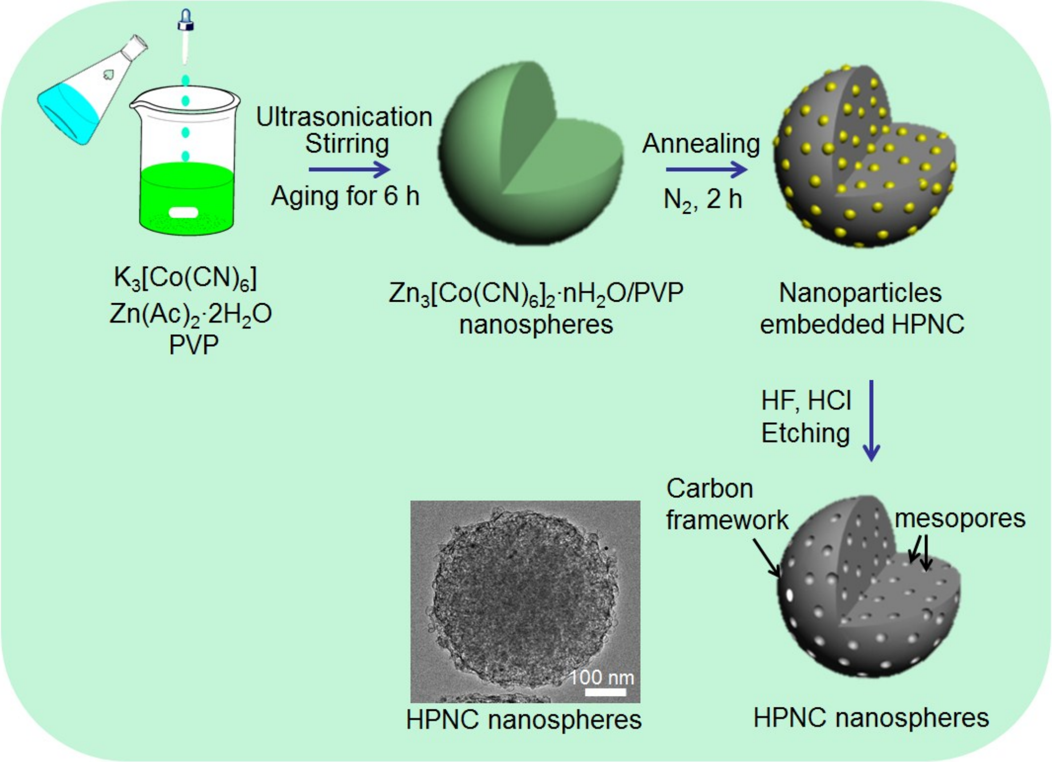

Fig. S1. Schematic illustration of the synthesis procedure of HPNC nanospheres.

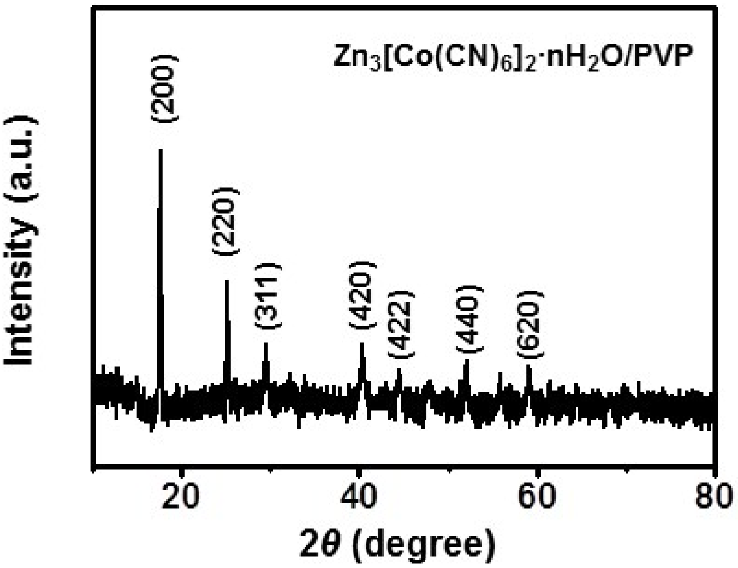

Fig. S2. X-ray diffraction (XRD) spectrum of the $Zn_3[Co(CN)_6]_2{\cdot}nH_2O$/PVP precursor nanospheres (JCPDS card No. 23-1494, space group: *Fm-3m*, *a* = 9.940, *b* = 9.940, *c* = 9.940).

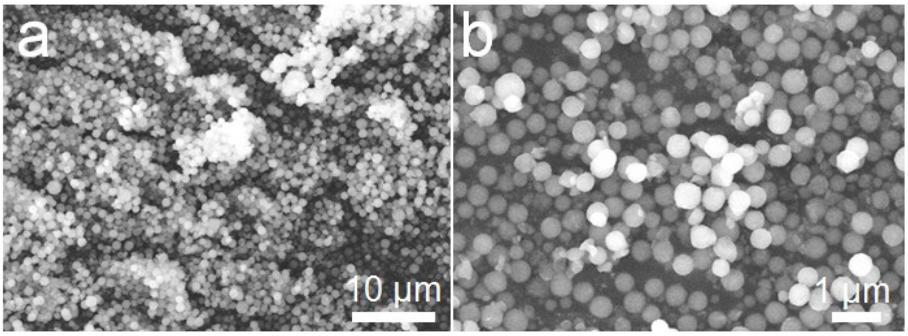

Fig. S3. (a,b) Field-emission scanning electron microscopy (FESEM) images of the $Zn_3[Co(CN)_6]_2{\cdot}nH_2O$/PVP precursor nanospheres. Uniform distributed nanospheres with the diameter range of 500–700 nm can be seen clearly.

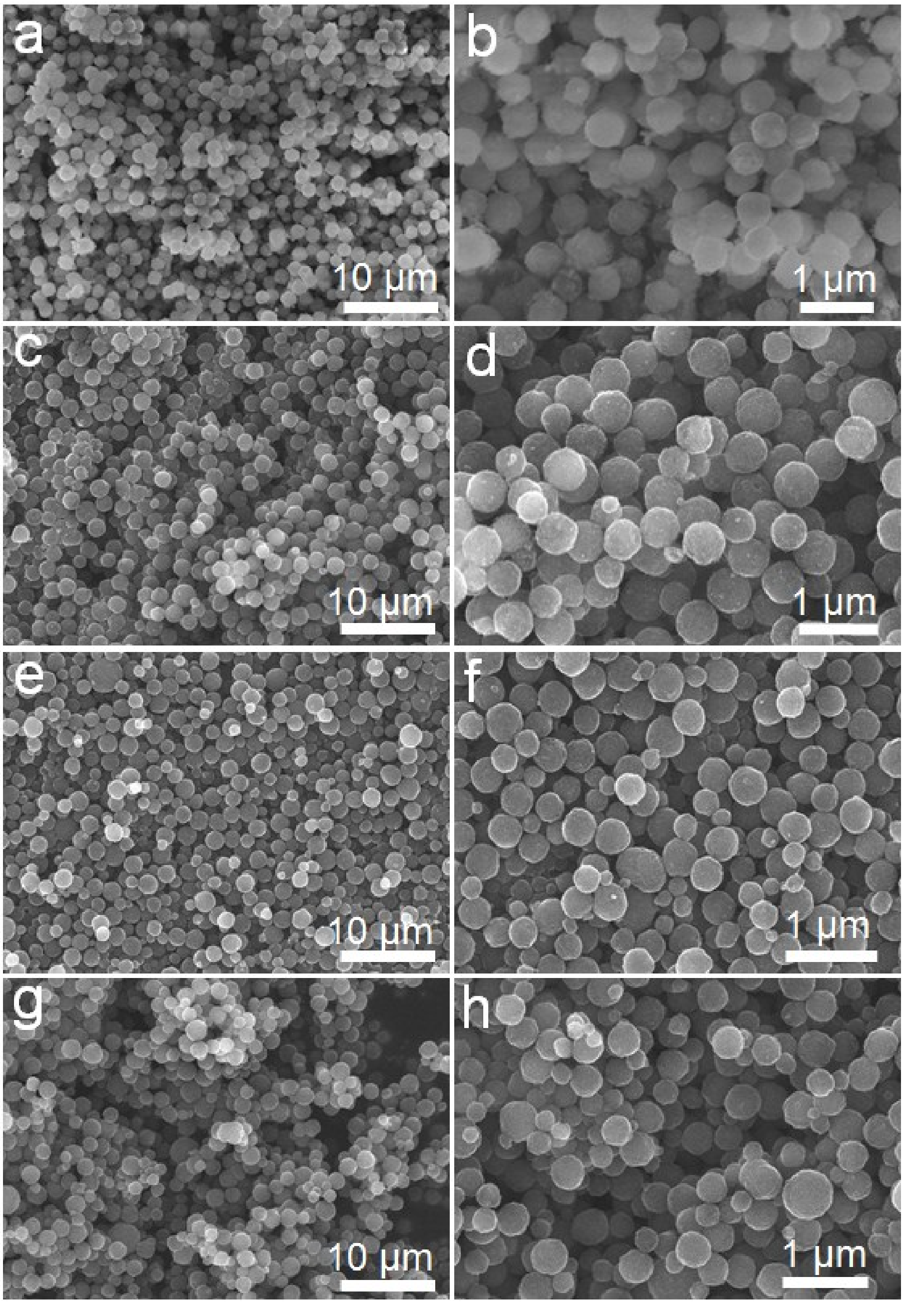

Fig. S4. FESEM images of the $Zn_3[Co(CN)_6]_2 \cdot nH_2O$/PVP precursor nanospheres after thermal annealing at (a,b) 500 °C, (c,d) 600 °C, (e,f) 700 °C, and (g,h) 800 °C, respectively. All the products inherited the spherical morphology but with shrinked diameter (400−500 nm).

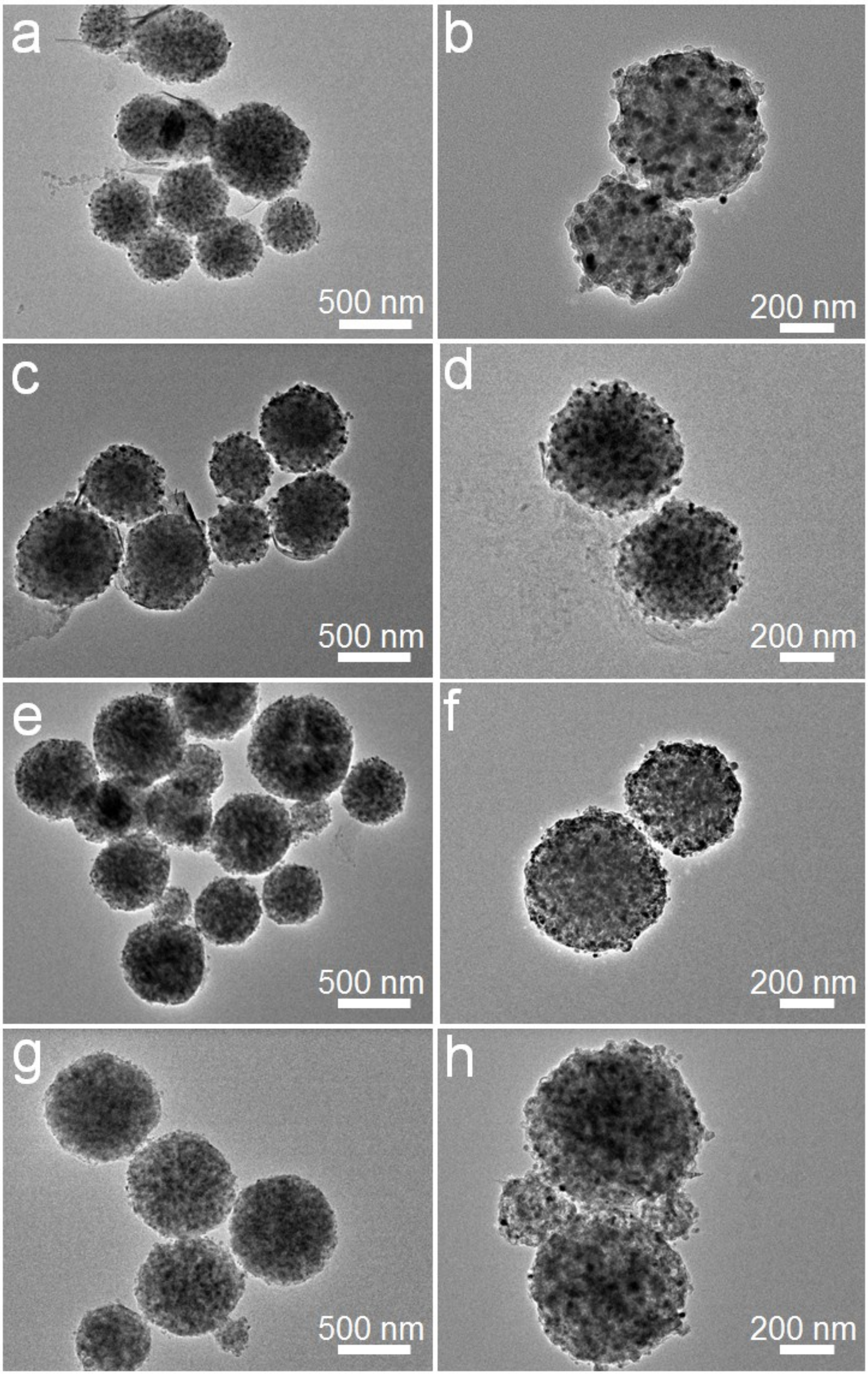

Fig. S5. Transmission electron microscopy (TEM) images of the carbide/carbon nanospheres derived from $Zn_3[Co(CN)_6]_2{\cdot}nH_2O$/PVP precursor nanospheres after thermal annealing at (a,b) 500 °C, (c,d) 600 °C, (e,f) 700 °C, and (g,h) 800 °C, respectively. All the products display similar morphology with nanoparticles embedded into carbon frameworks.

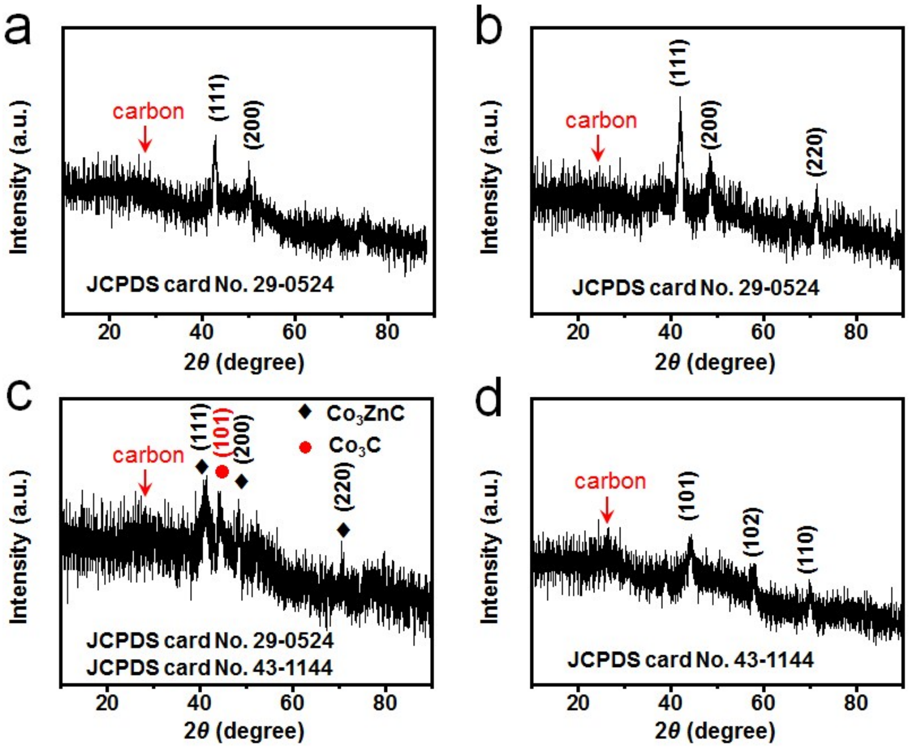

Fig. S6. XRD spectra of the carbide/carbon nanospheres derived from $Zn_3[Co(CN)_6]_2 \cdot nH_2O$/PVP precursor nanospheres after thermal annealing at (a) 500 °C, (b) 600 °C, (c) 700 °C, and 800 °C. The diffraction peaks of Co_3ZnC can be clearly recognized in the XRD spectra of (a) and (b) (JCPDS card No. 29-0524, space group: *Pm-3m*, $a = 3.730$, $b = 3.730$, $c = 3.730$). The XRD diffraction peaks in (c) can be attributed to the co-existence of Co_3ZnC and Co_3C (JCPDS card No. 43-1144, space group: *P63/mmc*, $a = 2.685$, $b = 2.685$, $c = 4.335$). The formation of Co_3C can be ascribed to the gradual evaporation of Zn element in Co_3ZnC. The XRD diffraction peaks in (d) are totally attributed to the Co_3C, because Zn element in the product has been evaporated thoroughly. Therefore, it can be concluded that with the increase of thermal annealing temperature from 500 to 800 °C, the embedded carbide nanoparticles evolved from Co_3ZnC to Co_3C.

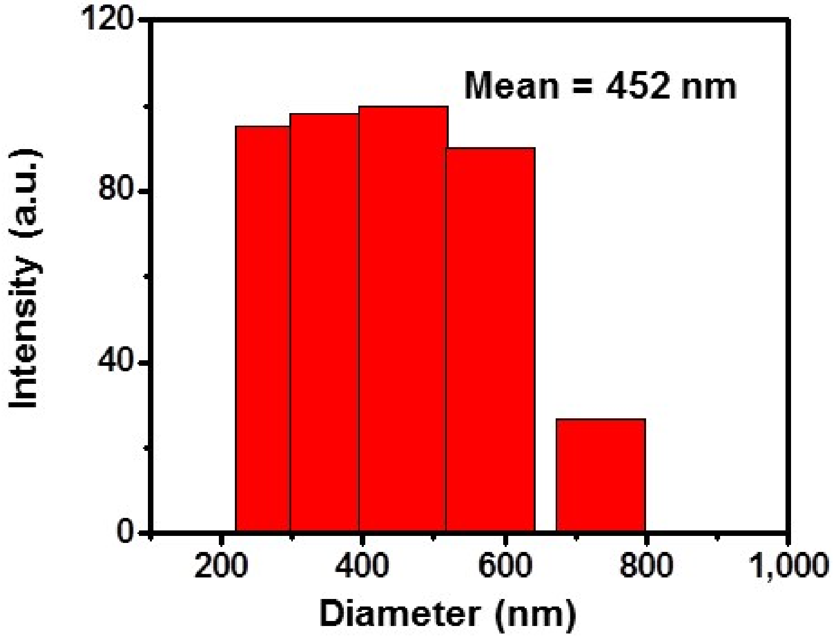

Fig. S7. Dynamic light scattering (DLS) analysis of HPNC-*600* nanospheres.

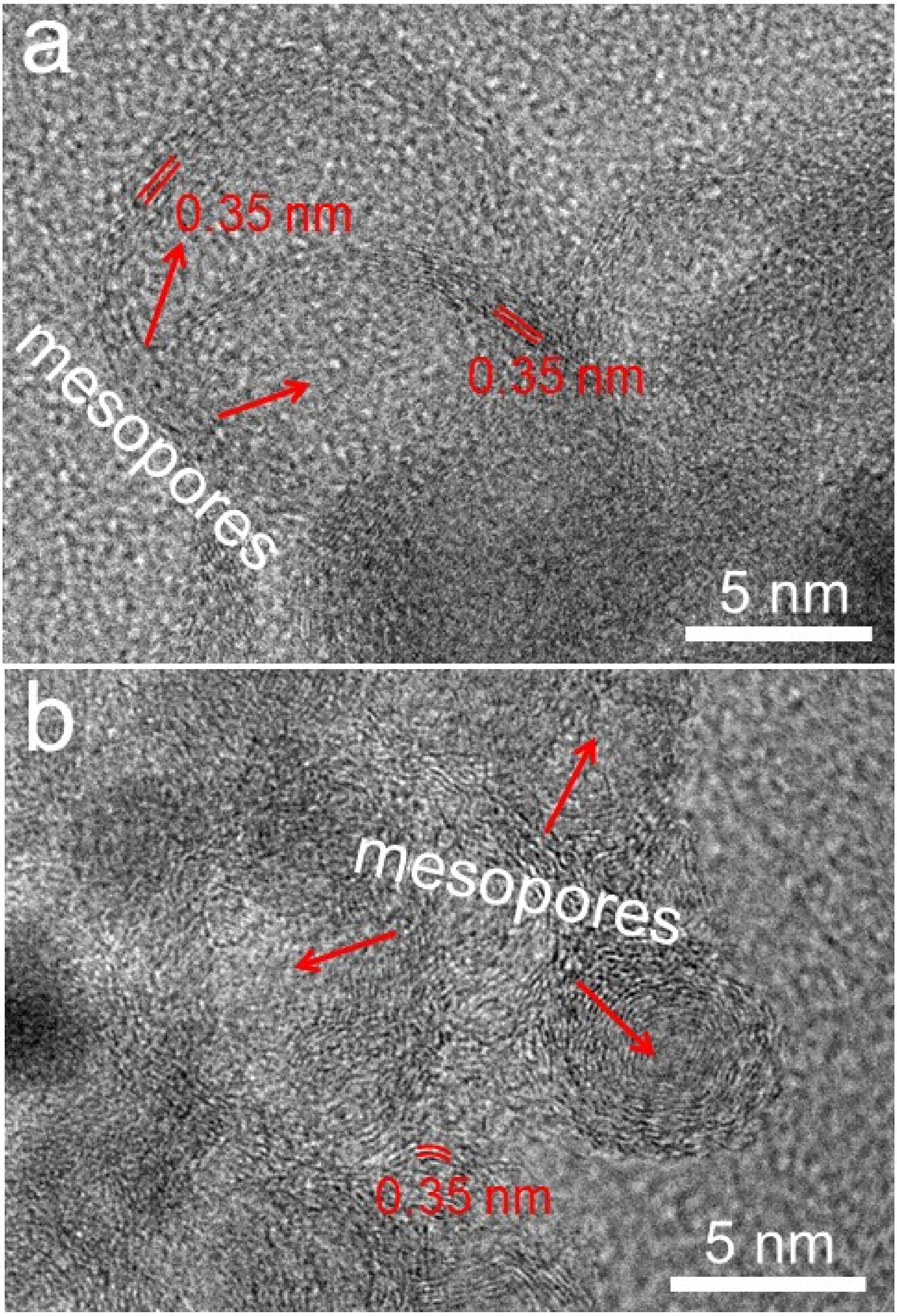

Fig. S8. (a,b) High-resolution transmission electron microscopy (HRTEM) images of HPNC-*600* nanosphere. The HRTEM observations clearly revealed the existence of mesopores, as marked with red arrows. The observed lattice distances correspond to the (002) plane of graphite but with a larger value (0.35 nm).

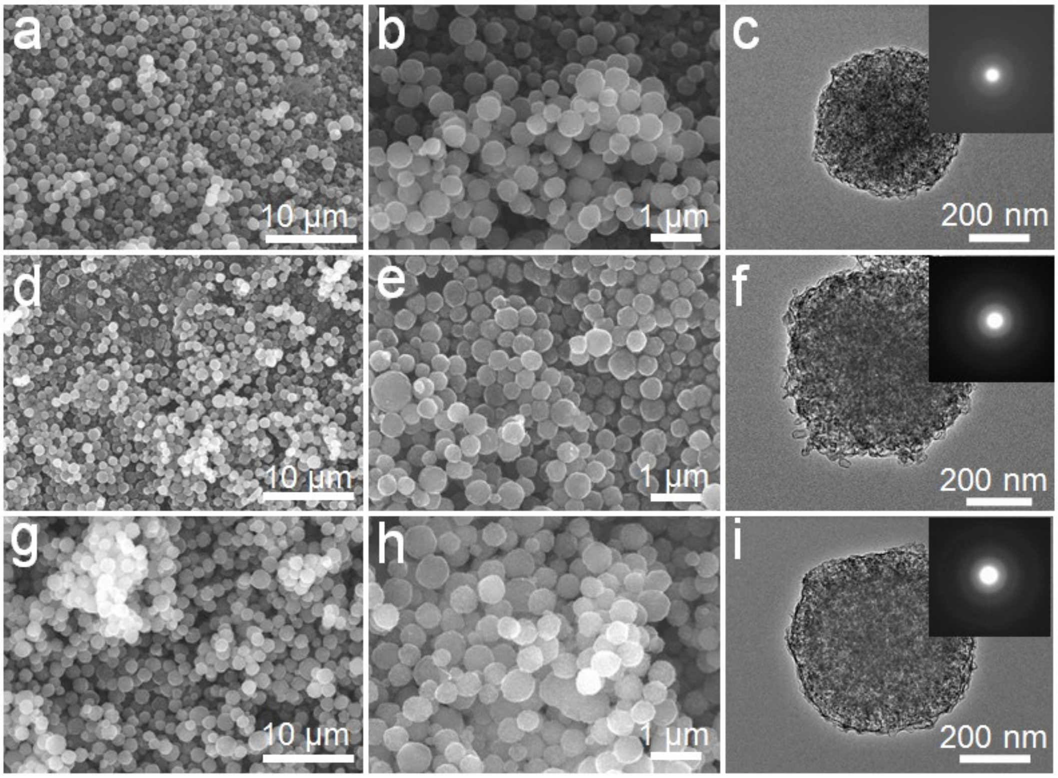

Fig. S9. (a,b) FESEM and (c) TEM images of HPNC-*500* nanospheres. (d,e) FESEM and (f) TEM images of HPNC-*700* nanospheres. (g,h) FESEM and (i) TEM images of HPNC-*800* nanospheres. The insets of (c), (f), and (i) show the selected-area electron diffraction (SAED) patterns of HPNC-*500*, HPNC-*700*, and HPNC-*800* nanospheres, respectively. These images reveal the similar morphology and nanostructure to that observed from HPNC-*600* nanospheres.

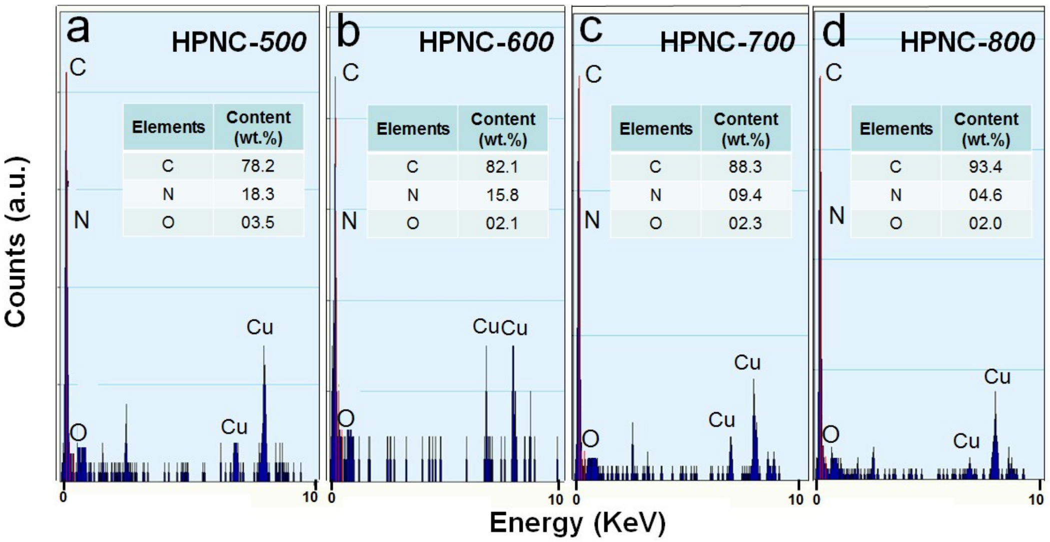

a

Elements	Content (wt.%)
C	78.2
N	18.3
O	03.5

b

Elements	Content (wt.%)
C	82.1
N	15.8
O	02.1

c

Elements	Content (wt.%)
C	88.3
N	09.4
O	02.3

d

Elements	Content (wt.%)
C	93.4
N	04.6
O	02.0

Fig. S10. Energy dispersive X-ray (EDX) spectra of (a) HPNC-*500*, (b) HPNC-*600*, (c) HPNC-*700*, and (d) HPNC-*800*.

Table S3. Brunauer–Emmett–Teller (BET) parameters of HPNC samples determined by the nitrogen adsorption-desorption isotherms.

Samples	**Specific surface area (m^2/g)**	**Total pore volume (cm^3/g)**	**Average diameter of micropores (nm)**	**Size range of mesopores (nm)**
HPNC-*500*	274.4	0.35	1.0	3.0–12
HPNC-*600*	531.5	0.81	1.1	3.0–15
HPNC-*700*	394.6	0.64	1.0	3.0–15
HPNC-*800*	426.9	0.70	0.9	3.0–15

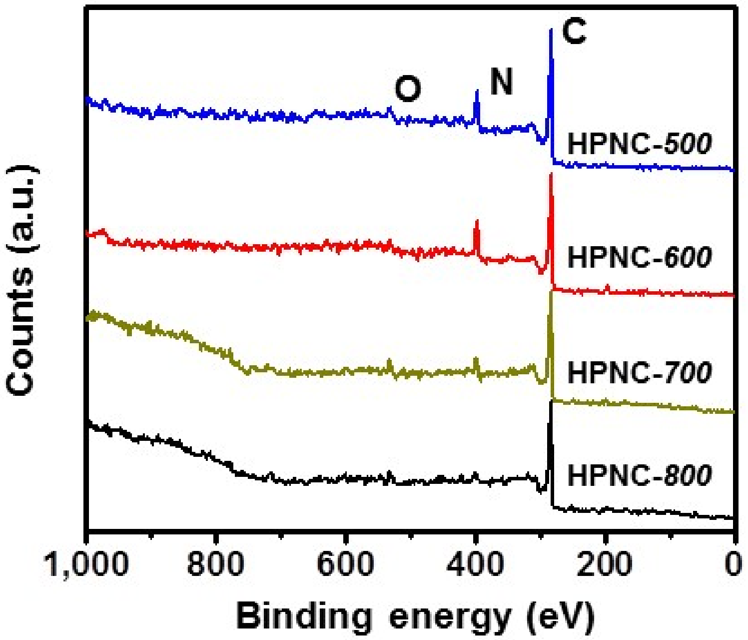

Fig. S11. Survey X-ray photoelectron spectroscopy (XPS) spectra of HPNC samples.

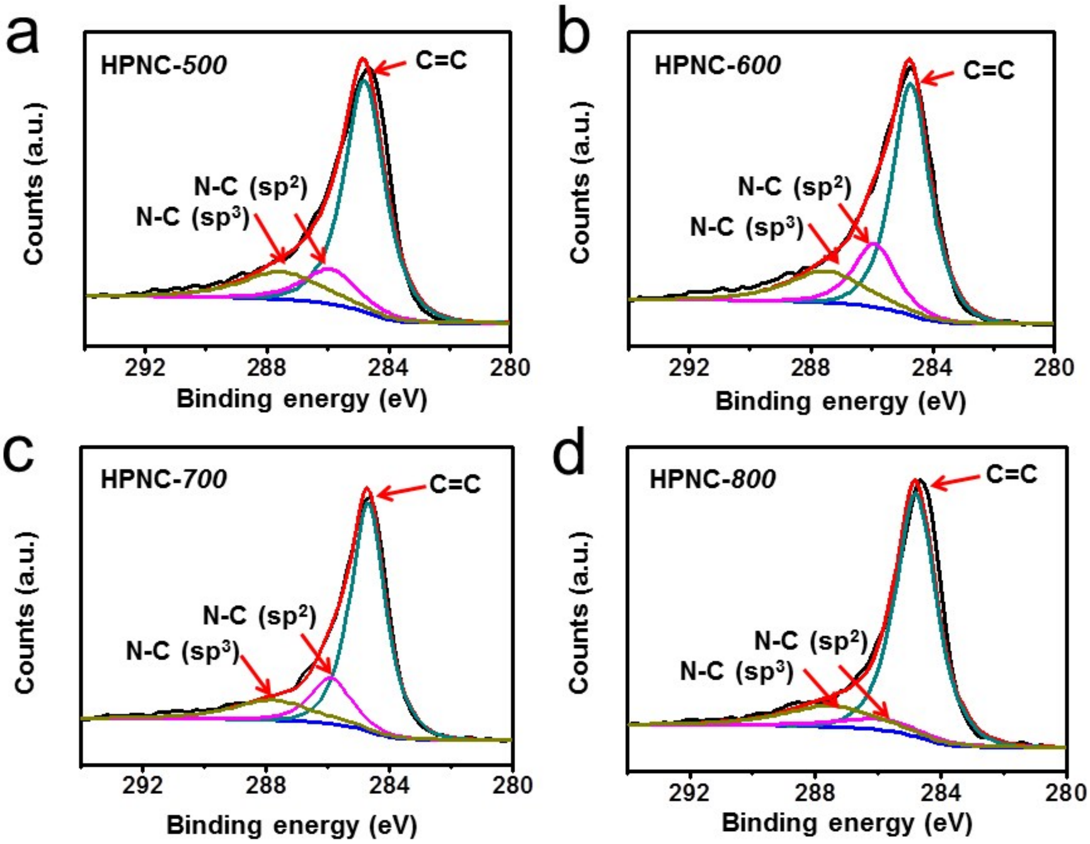

Fig. S12. The high-resolution XPS spectra of C 1s regions of (a) HPNC-*500*, (b) HPNC-*600*, (c) HPNC-*700*, and (d) HPNC-*800* nanospheres, respectively.

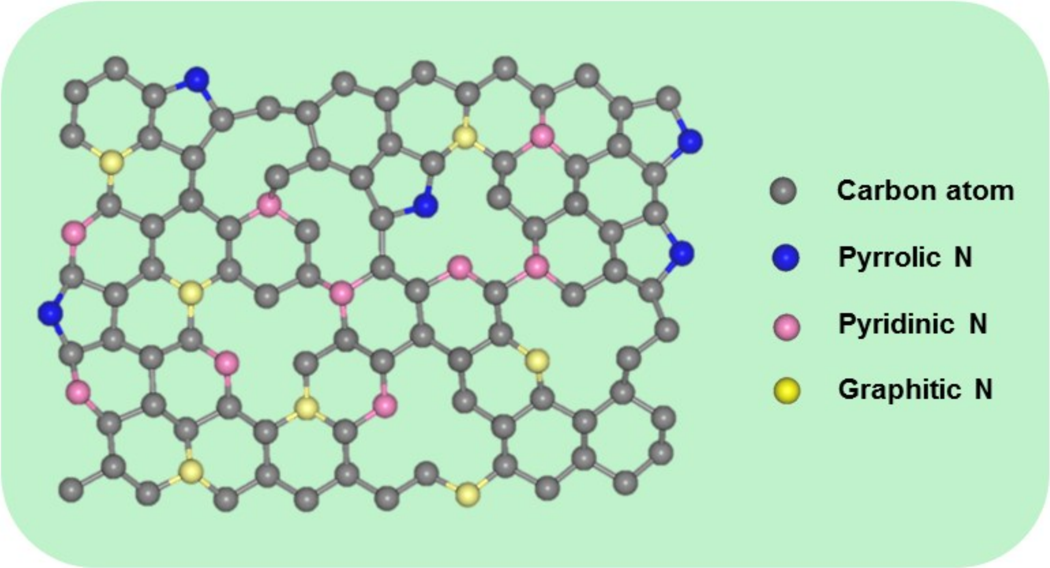

Fig. S13. Schematic illustration of the atomic structure of nitrogen-rich carbon layer in HPNC samples.

Table S4. The parameters of XPS spectra and the fitting results of N 1s peaks of HPNC samples.

Samples	**XPS (wt.%)**			**#Percentage of total N 1s**		
	C	**N**	**O**	**graphitic N**	**pyrrolic N**	**pyridinic N**
HPNC-*500*	77.5	19.3	3.2	16.1	38.8	45.1
HPNC-*600*	80.2	17.4	2.4	21.0	35.6	43.4
HPNC-*700*	87.2	10.6	2.2	34.4	24.9	40.7
HPNC-*800*	92.9	5.1	2.0	40.8	25.6	33.6

The percentage of different nitrogen species in total N 1s were determined based on the deconvoluted XPS spectra of HPNC samples.

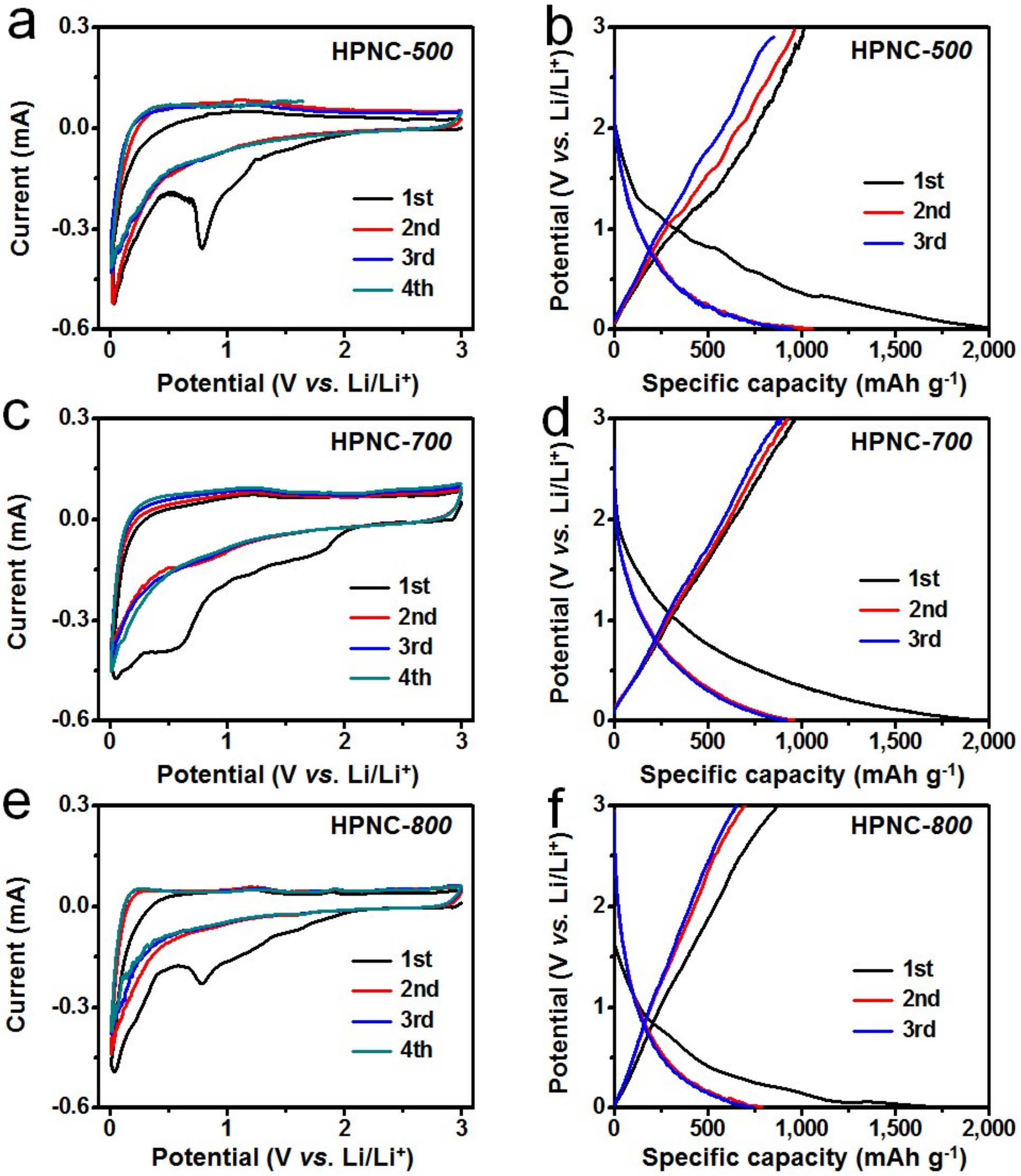

Fig. S14. Lithium storage performance of HPNC samples. Typical CV curves (a) and charge-discharge profiles (b) of HPNC-*500* based anode. Typical CV curves (c) and charge-discharge profiles (d) of HPNC-*700* based anode. Typical CV curves (e) and charge-discharge profiles (f) of HPNC-*800* based anode.

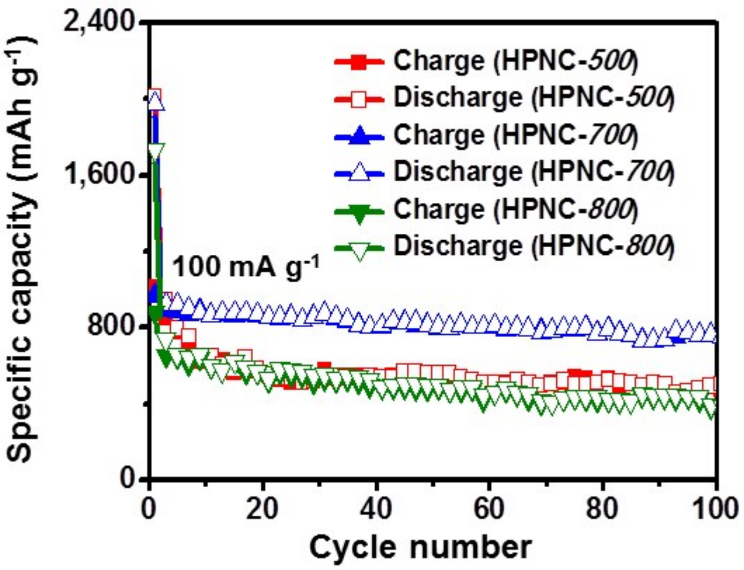

Fig. S15. Cycling performance of HPNC-*500*, HPNC-*700*, and HPNC-*800* based anodes for LIBs at 100 mA g^{-1}.

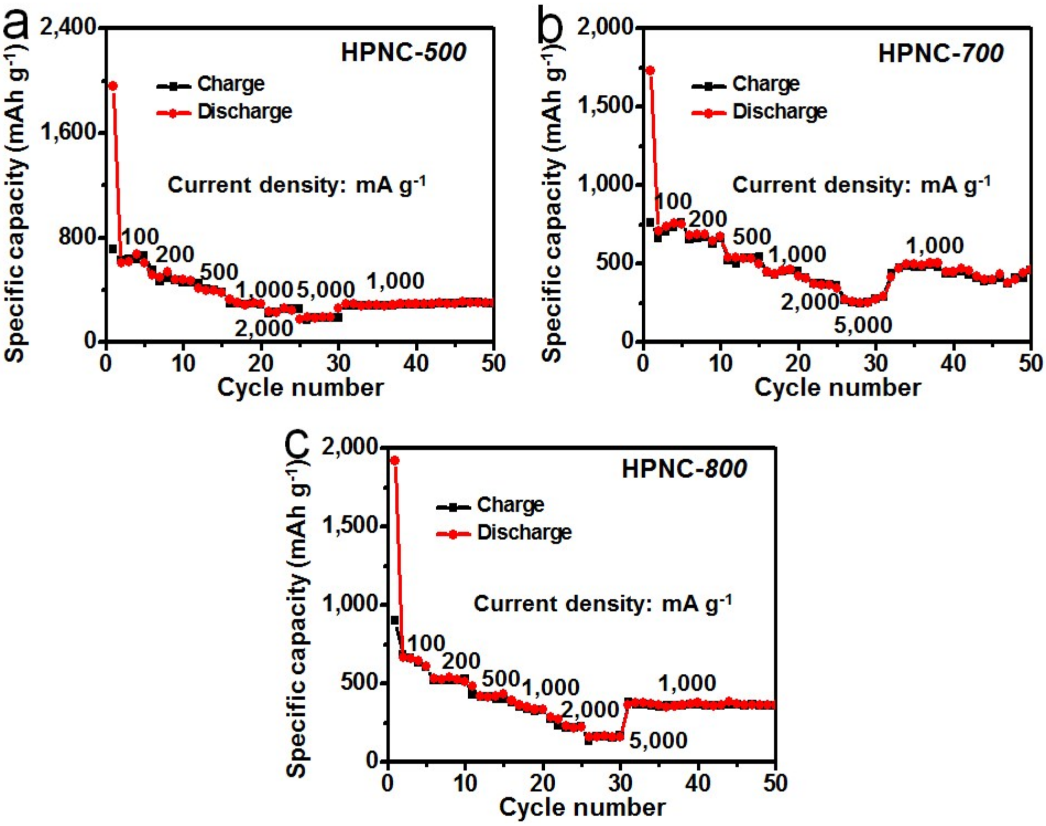

Fig. S16. Rate performances of (a) HPNC-*500*, (b) HPNC-*700*, and (c) HPNC-*800* based anodes for LIBs at various current densities (100–5,000 mA g^{-1}).

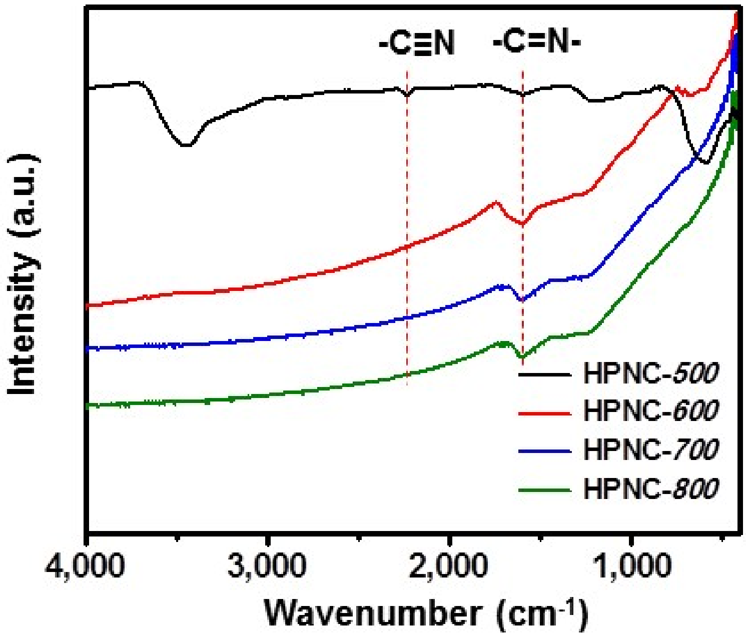

Fig. S17. Fourier transform infrared (FT-IR) spectra of HPNC samples. The band at about 2225 cm^{-1} is attributed to the cyan groups (–C≡N), and the band at about 1600 cm^{-1} belongs to the stretching vibration of –C=N– bonds. Both the bands at 2225 and 1600 cm^{-1} can be observed clearly in the spectrum of HPNC-*500*, suggesting that the –C≡N groups are still existed in HPNC-*500* nanospheres. However, the band of –C≡N disappeared and the band intensity of –C=N– bonds increased in the FT-IR spectra of HPNC-*600*, HPNC-*700*, and HPNC-*800* samples, indicating that the –C≡N groups were removed thoroughly in these samples by high-temperature annealing.

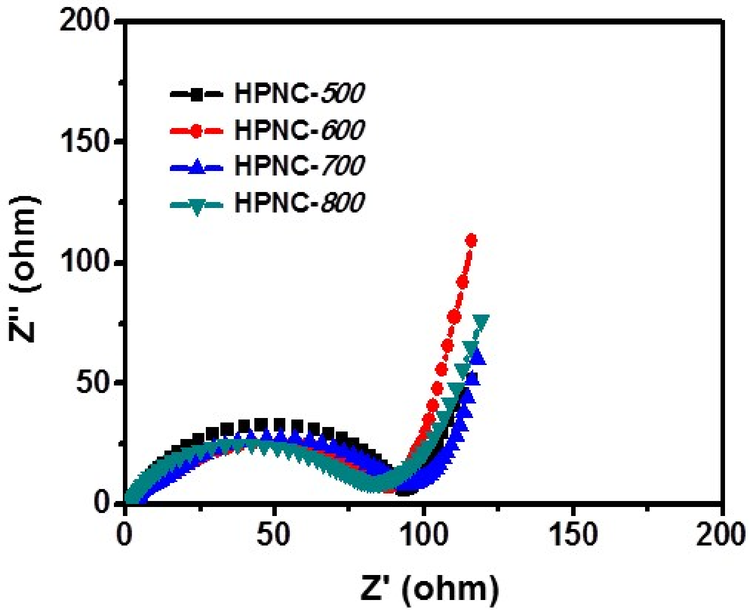

Fig. S18. Nyquist plots of HPNC based anodes for LIBs.

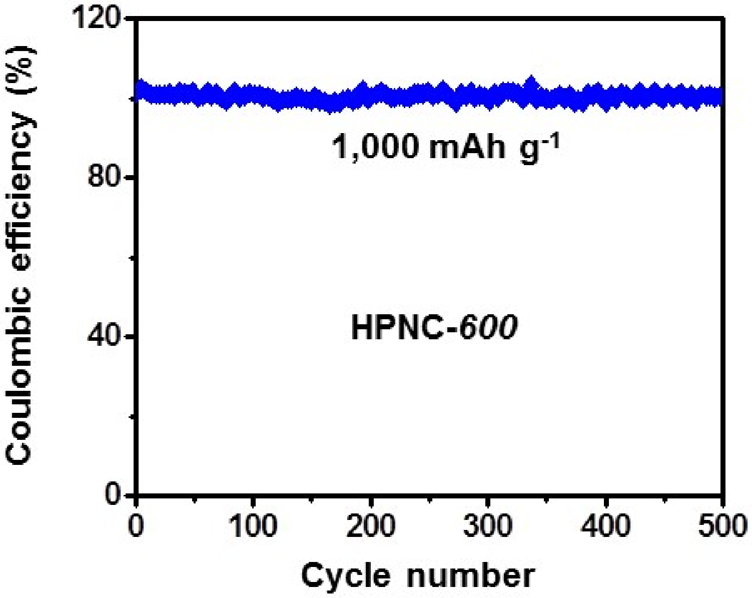

Fig. S19. The Coulombic efficiency of HPNC-*600* based anode for LIBs within the first 500 cycles at 1,000 mA g^{-1}.

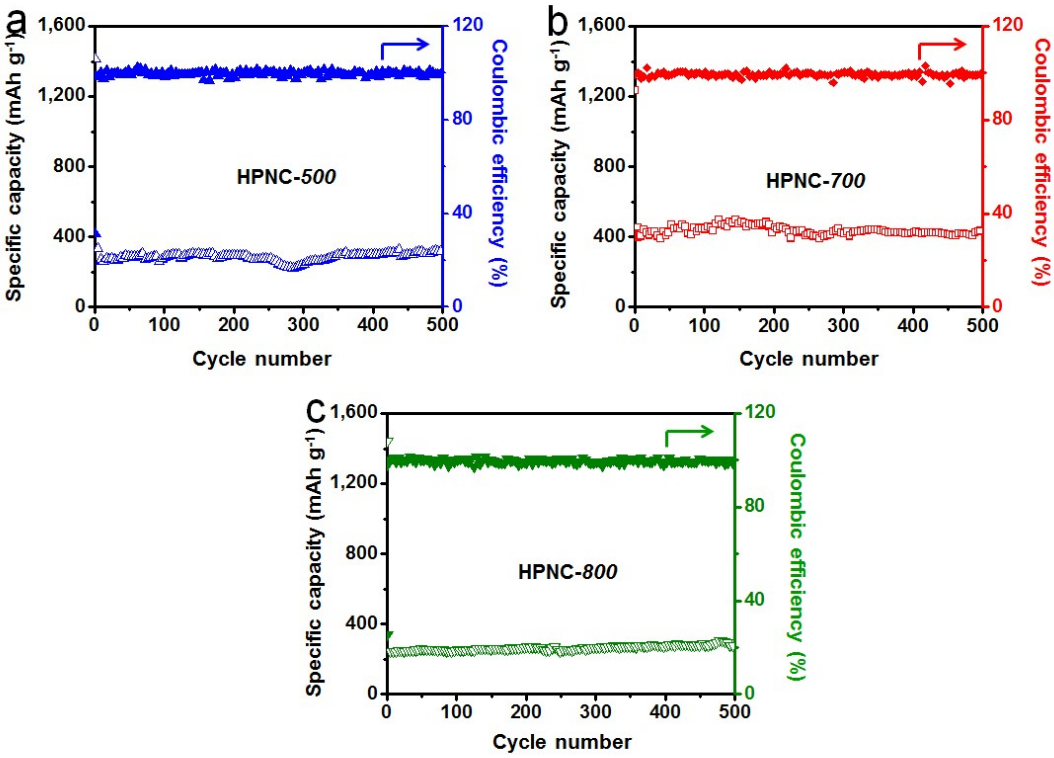

Fig. S20. Cycling performances and corresponding Coulombic efficiencies of (a) HPNC-*500*, (b) HPNC-*700*, and (c) HPNC-*800* based anodes for LIBs at 1,000 mA g^{-1}.

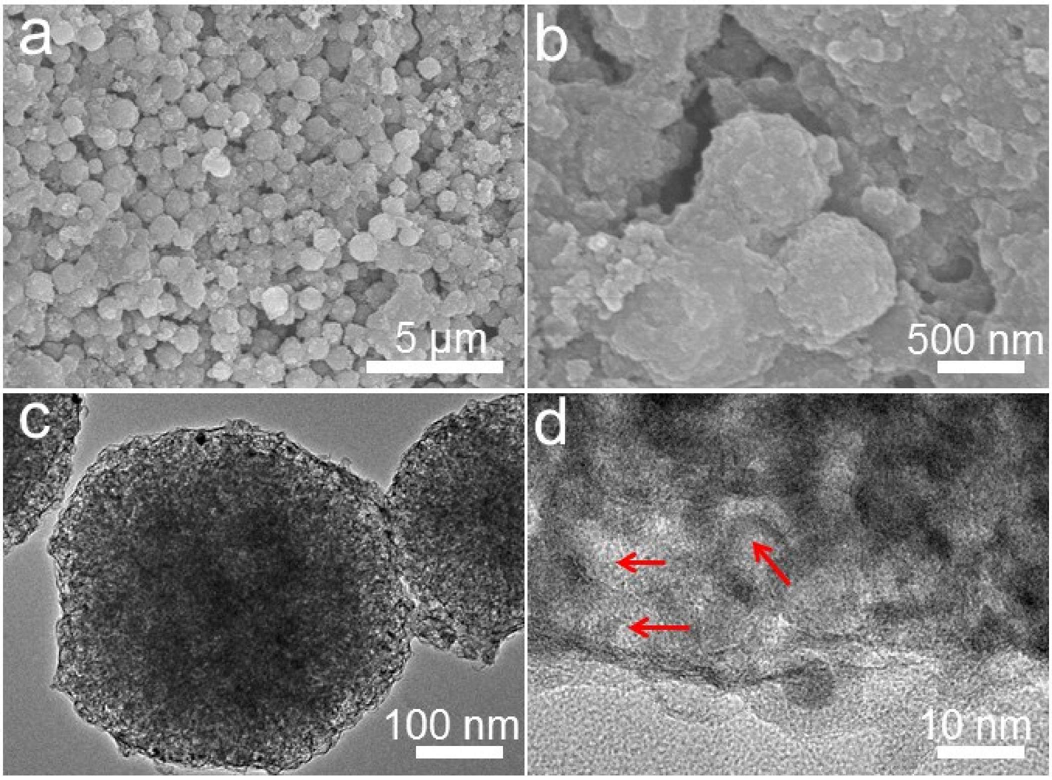

Fig. S21. (a,b) FESEM and (c,d) TEM images of HPNC-*600* nanospheres after long-term stability tests (1,000 cycles) at 5,000 mA g^{-1} for LIBs. The red arrows in (d) indicate the existence of mesopores in HPNC nanospheres. The FESEM and further TEM characterizations reveal that the morphology of HPNC-*600* nanospheres retains well even after long-term cycling at a very high current density.

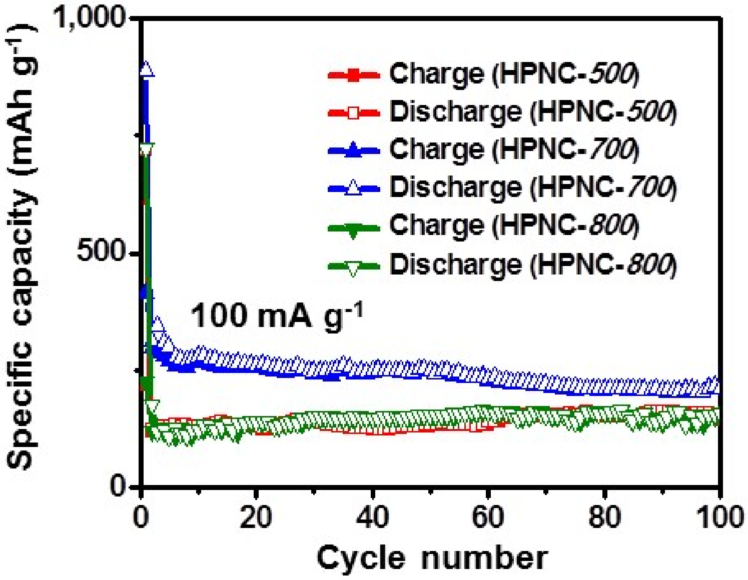

Fig. S22. Cycling performance of HPNC-*500*, HPNC-*700*, and HPNC-*800* based anodes for SIBs at 100 mA g^{-1}.

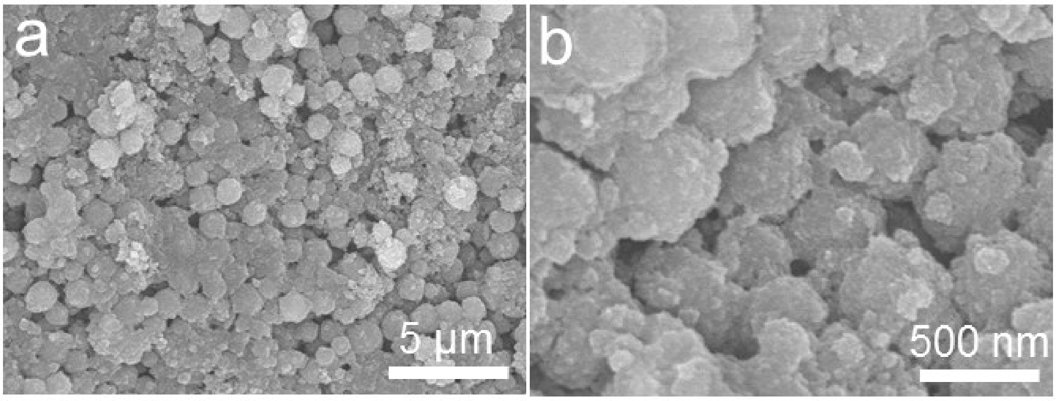

Fig. S23. (a,b) FESEM images of HPNC-*600* nanospheres after long-term cycling stability tests (500 cycles) at 1,000 mA g^{-1} for SIBs.